Microfluidic Processing Approach to Controlling Drug Delivery Properties of Curcumin-Loaded Block Copolymer Nanoparticles

Ruyao Chen, Jeremy E. Wulff, & Matthew G. Moffitt

September 2018

https://doi.org/10.1021/acs.molpharmaceut.8b00529

A Microfluidic Processing Approach to Controlling Drug Delivery Properties of Curcumin-Loaded Block Copolymer Nanoparticles

Ruyao Chen, Jeremy E. Wulff and Matthew G. Moffitt*

Department of Chemistry, University of Victoria, P.O. Box 3065, Victoria, BC, Canada V8W 3V6

Abstract

We apply gas-liquid microfluidic reactors containing flow-variable, high-shear "hot spots" to produce curcumin-loaded polymer nanoparticles (CUR-PNPs) comprised of poly(caprolactone)-*block*-poly(ethylene oxide) (PCL-*b*-PEO) block copolymers at various flow rates and CUR loading ratios. CUR-PNPs prepared using the conventional nanoprecipitation method (bulk method) showed decreased encapsulation efficiency and increased drug precipitation as the loading ratio increased. However, CUR-PNPs prepared by microfluidic manufacturing showed both increased encapsulation efficiency and increased drug loading as either the flow rate or the loading ratio increased. This enabled microfluidic CUR loading percentages of up to 30 % to be achieved in this study, which to our knowledge is a record for block copolymer PNPs. As well, it is shown that increased flow rate of microfluidic manufacturing leads to decreased mean CUR-PNP sizes (down to ~50 nm) and narrower size distributions, along with significantly different CUR release kinetics compared to CUR-PNPs prepared at slower flow rates. *In vitro* antiproliferation experiments against MDA-MB-231 cells give an average IC_{50} value of 24 μM for CUR-PNPs compared to 13 μM for free CUR at the same incubation time of 72 h. Compared to conventional bulk and single-phase microfluidic strategies, this unique two-phase reactor represents an exciting manufacturing platform for optimizing polymeric CUR nanomedicines though flow-directed shear processing.

Keywords: drug delivery, microfluidics, polymer nanoparticles, curcumin

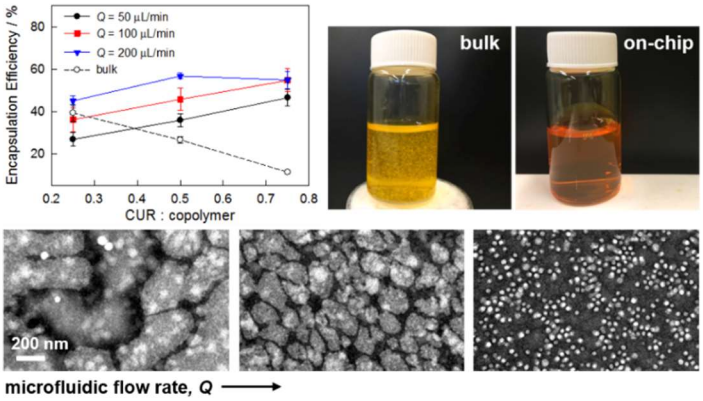

Introduction

Many important anticancer therapeutics are both hydrophobic and non-selective, requiring specific formulation in order to achieve good bioavailability and to mitigate side effects.[1] Polymer nanoparticles (PNPs) formed from amphiphilic block copolymers are capable of encapsulating various hydrophobic drugs within their cores, thus increasing aqueous dispersibility and bioavailability.[2-21] As well, the nanoscale sizes of drug-loaded PNPs (10-100 nm) enable their passive localization in cancerous tumours *via* the enhanced permeability and retention (EPR) effect, effectively increasing selectivity of the encapsulated therapeutic agent.[2, 12] Additional opportunities for active targeting can be achieved by chemical conjugation of specific target molecules, including folic acid, galactose, arginine-glycine-aspartic acid tripeptide (RGD), and biotin, to the PNP coronal chains.[12, 14, 18, 22, 23] A wide variety of PNP materials, including poly(D,L-lactide)-*block*-poly(ethylene oxide) (PDLLA-*b*-PEO),[24] poly(lactide-*co*-glycolic acid)-*block*-poly(ethylene oxide) (PLGA-*b*-PEO),[25] polycaprolactone-*block*-poly(ethylene oxide) (PCL-*b*-PEO),[26] poly(methyl caprolactone-*co*-caprolactone)-*block*-poly(ethylene oxide) (P(MCL-*co*-CL)-*b*-PEO)[27] and poloxamers (Pluronics®)[28] have been widely studied for drug delivery applications. Compared to other nanomedicine formulations, including liposomes and lipid nanoparticles, these block copolymer-based systems offer distinct advantages of high stability, diversity of properties, and ease of chemical functionalization.[2, 4, 19]

Curcumin (CUR) is a polyphenolic compound extracted from the turmeric root (*Cumera longa*) which has been used for centuries as a spice, colorant, and therapeutic agent in traditional Asian medicine.[29] In recent years, scientific interest in CUR has increased rapidly, due to a large number of studies reporting its beneficial therapeutic properties as an anti-oxidant and anti-inflammatory agent.[30, 31] In addition, CUR has shown promising anticancer activity attributed to

inhibition of several transcription factors, including NF-κB, AP-1, STAT-1 and STAT-3, involved in proliferation and survival of cancer cells.[29, 31-33] However, impeding the medical applications of CUR are its extremely poor aqueous solubility in addition to its chemical instability at physiological pH, leading to poor bioavailability and ineffective delivery to target sites.[33, 34] While some researchers have argued that the medical potential of CUR has been overstated,[34] it is generally recognized that any beneficial medicinal properties of CUR can only be exploited if the aforementioned challenges are mitigated by appropriate formulation.[33, 35, 36]

In response to these challenges, numerous researchers have investigated CUR encapsulation in the hydrophobic cores of block copolymer PNPs.[36-55] These studies have shown that CUR encapsulation promotes improved aqueous dispersion, increased chemical stability, and more sustained release compared to free CUR. *In vivo* studies have additionally shown that CUR-loaded PNPs (CUR-PNPs) show enhanced bioavailability, improved distribution in the body, and promising antitumor activity compared to the unencapsulated drug.[39, 47, 54] CUR-PNPs are typically prepared using conventional self-assembly approaches, such as nanoprecipitation, thin film hydration, or dialysis, in which intermolecular forces alone are responsible for the size, structure, and drug delivery properties of the resulting colloids. In order to modulate intermolecular forces and change the final product using these methods, changes must be made to the chemistry of the formulation (block copolymer molecular weight or composition, solvent, drug, or drug-to-polymer loading ratio), often within a narrow window of requirements for the particular pharmaceutical application. A survey of the literature points to a number of inherent limitations of these conventional methodologies for CUR encapsulation. First, CUR is a therapeutic agent with relatively high IC_{50} values compared to other anticancer drugs,[36] such that formulations with large amounts of CUR compared to excipients should be advantageous; however, current drug loadings

(*DL*) of CUR-PNPs range from ~2-20%,[37-45, 47, 49, 51-53] with no examples of *DL* > ~20% to our knowledge. Second, although increases in *DL* can be achieved by increasing the loading ratio (*r* = total mass CUR / mass copolymer), increases in *r* are generally accompanied by decreases in the encapsulation efficiency (*EE*) and concomitant increases in the amount of unencapsulated, precipitated CUR.[37, 38, 45, 47, 53] Third, mean sizes and polydispersities of CUR-PNPs are critical factors in their passive localization within tumors;[55] however, changes in the CUR loading ratio generally lead to changes in PNP size distributions, precluding *a priori* size control independent of CUR loading levels.[37, 40, 43, 47, 53] Finally, CUR release kinetics from CUR-PNPs are typically determined exclusively by the choice of polymer and the amount of drug, such that CUR release profiles cannot be tuned independently of these two parameters.[37-45, 47, 49, 51-53]

In contrast to such bottom-up methods, a novel approach to producing drug delivery PNPs is to apply external mechanical forces such as shear to act in tandem with intermolecular forces, allowing structure and properties to be tuned using external experimental handles without changing the chemistry of the formulation. This strategy for tuning polymer material properties, generally known as "polymer processing", has been applied for many years in the engineering of commodity polymer products. For example, the stretching of extruded polyamide fibers will increase the alignment and weight fraction of crystallites leading to improved sheen and tensile strength of the resulting nylon material.[56] The translation of such polymer processing concepts to the nanoscale, such as the application of high shear as an external (or "top-down") force for modulating the structure and function of PNPs, offers exciting possibilities for tuning the properties of soft nanomaterials.[57] In our group, we have applied flow-variable, high-shear "hot spots" within two-phase, gas-liquid microfluidic reactors to manipulate the structure and properties of block copolymer colloids,[58-65] including drug-loaded PNPs,[27, 57, 66-68] independent of changes in

the drug, polymer or other formulation components. For example, using our microfluidic platform, we have encapsulated the anticancer drug paclitaxel (PAX) within PNPs consisting of various copolymers with PEO hydrophilic blocks and hydrophobic blocks of PCL[57, 66, 68] or P(MCL-*co*-CL).[27] We have demonstrated that variation in the flow rate of microfluidic manufacturing provides control and optimization of PNP sizes and morphologies,[27, 57, 66, 68] drug loading efficiencies,[27, 57, 66, 68] release rates,[27, 57, 66, 68] and antiproliferation effects against MCF-7 breast cancer cells,[27, 57] independent of chemical formulation parameters. Although many other, mostly single-phase, microfluidic strategies have been applied to the manufacturing of PNP nanomedicines,[69] including those for CUR delivery,[52, 70] none of these have demonstrated the processing control of PNP size and structure that is enabled by the high-shear "hot spots" within the microchannels of two-phase gas-liquid mixers.[27, 58, 59]

In this study, we demonstrate microfluidic shear processing control of the sizes, morphologies, loading, and release of CUR-PNPs. Consistent with previous studies,[37, 38, 45, 47, 53] we show that conventional nanoprecipitation manufacturing leads to decreased loading efficiencies and increased CUR precipitation as the amount of CUR in a formulation increases. In contrast, microfluidic manufacturing leads to CUR loading efficiencies that increase with both loading ratio and flow rate, allowing CUR loading of up to *D*L = 30 % to be achieved in this study. In addition, we show that increasing microfluidic flow rate decreases the mean size and polydispersity of CUR-PNP populations, providing processing control of particle populations within the EPR regime, independent of the amount of added CUR. For the same polymer and loading ratio, we also show that CUR release profiles can be tuned by changes in microfluidic flow rate. Finally, we demonstrate *in vitro* cytotoxicity effects of free CUR and CUR-PNPs prepared at various flow rates against the MDA-MB-231 breast cancer cell line. These results demonstrate the

potential of microfluidic shear processing for the control and optimization of PNP formulations for medical applications of CUR.

Experimental

Materials. PCL(12k)-*b*-PEO(5k) (PCL-*b*-PEO, numbers in brackets indicate number average molecular weights of the respective blocks) was purchased from Advanced Polymer Materials Inc (Montreal, Canada). Curcumin from *Curcuma longa* (Turmeric) (Product no: C1386) was purchased from Sigma-Aldrich. NaCl (EMD Inc), KCl (Caledon), Na_2HPO_4 (BioBasic) and KH_2PO_4(Caledon) were used to prepare PBS solution. Dimethylformamide (DMF) and acetonitrile were purchased from Caledon. Dialysis tubing with molecular weight cut-off of 6.8 kD was purchased from SpectrumLabs.

The MDA-MB-231 human breast adenocarcinoma cell line was generously provided by Dr. Christine Allen (University of Toronto, Toronto, Canada). Fetal Bovine Serum (FBS) and Dulbecco's Modified Eagle's Medium Nutrient Mixture F-12 HAM with 15 mM HEPES, $NaHCO_3$, pyridoxine and L-glutamine (DMEM) were purchased from Sigma Aldrich life science. The CellTiter-Blue cell viability assay kit was purchased from Promega. MDA-MB-231 cells were grown in a sterile tissue culture flask with a surface area of 75 cm^2. Sterile, 96-well flat-bottomed plates were purchased from Becton Dickinson Labware.

Bulk Preparation of CUR-PNPs. For comparison with microfluidic preparations, CUR-PNPs were formed by the conventional method of microprecipitation. For these experiments, ~5 g of 0.33 wt % copolymer solutions in DMF with various total added CUR/polymer (w/w) loading ratios (r = 0.25, 0.50 and 0.75) were prepared and equilibrated overnight. Then ~1 mL of stock solution was injected at a rate of 120 μL/min using a syringe pump into 10 × excess deionized

water with vigorous stirring. The resulting CUR-PNPs were then dialyzed (6-8 kD MWCO dialysis membrane, Spectrum Laboratories) against deionized water for 12 h to remove residual DMF, changing the deionized water every hour for the first 4 hours. The constant dialysis time and dialysis method applied to all bulk and microfluidic preparations allow meaningful comparison of encapsulation efficiencies even if small amounts of encapsulated CUR are removed with DMF during dialysis. Unencapsulated drug precipitate was removed from the dialyzed CUR-PNPs by centrifugation at 14000 × *g* for 5 minutes. After centrifugation, the supernatant was collected in a clean sample vial while the solid pellet was left in centrifugation vials. The solid pellet in each vial was washed by vortexing for 30 s with deionized water followed by centrifugation, then the supernatant from each wash was also collected in the sample vial. The washing step was repeated two more times. All samples were prepared in triplicate under the specified conditions. Experimentally determined characteristics of bulk-prepared CUR-PNPs are listed in *Supporting Information* (Table S1) and described in the text.

Microfluidic Reactor Fabrication. Negative masters were fabricated on silicon wafers (Silicon Materials) using the negative photoresist SU-8 100 (Microchem). A 150 μm-thick SU-8 film was spin-coated at 2000 rpm onto the silicon wafer and heated at 65 °C for 12 min and then at 95 °C for 50 min. After the wafer was cooled, a photomask was placed directly above and the wafer was exposed to UV light for 100 s. Then, the UV-treated film was heated at 65 °C for 1 min and then 95 °C for 20 min. Finally, the silicon wafer was submerged in SU-8 developer (Microchem) and rinsed with isopropanol until all unexposed photoresist was removed.

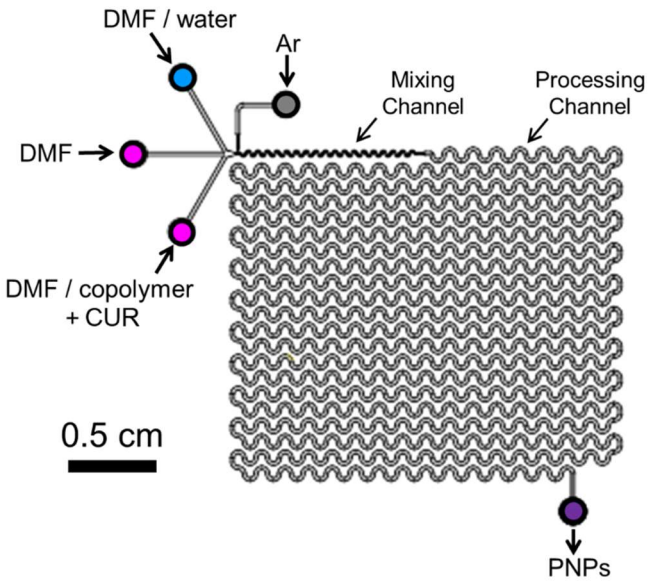

Figure 1. Schematic of two-phase gas-liquid microfluidic reactor. For all experiments, the gas-to-liquid flow ratio was ~1 and the on-chip water content was cwc + 10 wt %. The nominal total flow rate, Q, and the CUR/polymer (w/w) loading ratio, r, were varied in the experiments as described in the text.

Microfluidics chips were fabricated from poly(dimethyl siloxane) (PDMS) using a SYLGARD 184 silicon elastomer kit (Dow Corning). For fabrication of all PDMS chips, the elastomer and curing agent were mixed at a 7:1 ratio and degassed under vacuum. The resulting mixture was poured over a clean negative master chip in a Petri dish and further degassed until all remaining air bubbles were removed. The PDMS was heated at 85 °C until cured (~20 min), and then peeled from the negative master; holes were punched through the reservoirs of the resulting PDMS chip to allow for the insertion of tubing. A thin PDMS film (substrate layer) was also made on a glass slide by spin-coating a 20:1 elastomer / curing agent mixture followed by curing. The substrate layer was then permanently bonded to the base of the microfluidic reactor (channel layer) after both components were exposed to oxygen plasma for 45 s. The resulting reactor (Figure 1) has a set channel depth of 150 μm and consists of a sinusoidal mixing channel 100 μm wide and a

sinusoidal processing channel 200 μm wide, identical to the reactor described in previous publications from our group.

Flow Delivery and Control. Pressure-driven flow of liquids to the reactor inlet was provided using 1 mL gastight syringes (Hamilton, Reno, NV) mounted on syringe pumps (Harvard Apparatus, Holliston, MA). The microfluidic chip was connected to the liquid syringes *via* 1/16th-inch (OD) Teflon tubing (Scientific Products and Equipment, ON). Argon (Ar) gas flow was introduced to the chip *via* an Ar tank regulator and a downstream regulator (Johnston Controls) for fine adjustments. The chip was connected to the downstream regulator through a 1/16th-inch (OD) / 100-μm (ID) Teflon tube (Upchurch Scientific, Oak Harbor, WA). The liquid flow rate (Q_{liq}) was programmed *via* the syringe pumps and the gas flow rate (Q_{gas}) was fine-tuned *via* the downstream pressure regulator in order to set the nominal total flow rates (Q) of 50, 100, 200 and 400 μL/min described in the main text. Due to the compressible nature of the gas and the high gas/liquid interfacial tension, discrepancies arise between the nominal (programmed) and actual values of Q_{gas}, Q_{gas}/Q_{liq}, and the total flow rate (Q_{total}). Therefore, actual values of Q_{gas}, Q_{gas}/Q_{liq} and $Q_{total} = Q_{gas} + Q_{liq}$ for each microfluidic experiment (*Supporting Information*, Table S2) were calculated from the frequency of bubble formation and the average volume of gas bubbles, determined from image analysis of the mean lengths of liquid and gas plugs, L_{liq} and L_{gas}, respectively, under a given set of flow conditions. This method of flow calculation has been previously described by our group.[59] For all experiments, the relative gas-to-liquid flow ratio, Q_{gas}/Q_{liq} ~1 and all actual Q_{total} values are within 10% of nominal Q values reported in the main text.

Visualization of the gas bubbles and liquid plugs within the microfluidic reactor was achieved using an upright optical microscope (Omax) with a 10× objective lens. Images were

captured using a 2.07 megapixel PupilCam camera (Ken-A-Vision) and mean lengths of liquid and gas plugs were determined from the images using image analysis software (ImageJ).

Microfluidic Preparation of CUR-PNPs. For microfluidic preparation of CUR-PNPs, the following three fluid streams were combined to form gas-segmented liquid plugs within the reactor: (1) 1.0 wt % PCL-*b*-PEO solution in DMF with CUR/polymer loading ratios of r = 0.25, 0.50 and 0.75 (2) pure DMF, and (3) DMF/water. The flow rates of the three liquid streams were equal for all runs and the water content of the DMF/water stream was selected to yield steady state on-chip concentrations of 0.33 wt % copolymer and 15.5 wt % water. The critical water content of 0.33 wt % copolymer in DMF was previously determined to be 5.5 wt %,[66] so that the water content for microfluidic CUR-PNP preparation is designated cwc + 10 wt %.

For each CUR-PNP preparation, the sample was collected from the chip into vials containing 10× excess by volume of deionized water. The exceptions were CUR-PNPs for CUR release measurements, which were collected into vials containing 20× excess by volume of deionized water; the more dilute dispersions maintained better colloidal stability for longer-term release measurements. Following collections, CUR-PNPs were dialyzed (6-8 kD MWCO dialysis membrane, Spectrum Laboratories) against deionized water for 12 hours to remove residual DMF, changing the deionized water every hour for the first 4 hours. The constant dialysis time and dialysis method applied to all bulk and microfluidic preparations allow meaningful comparison of encapsulation efficiencies even if small amounts of encapsulated CUR are removed with DMF during dialysis. Unencapsulated drug precipitate was removed from the dialyzed CUR-PNPs by centrifugation at 14000 × g for 5 minutes. After centrifugation, the supernatant was collected in a clean sample vial while the solid pellet was left in centrifugation vials. The solid pellet in each vial was washed by vortexing for 30 s with deionized water followed by centrifugation, then the

supernatant from each wash was also collected in the sample vial. The washing step was repeated two more times. All samples were prepared in triplicate under the specified conditions. Experimentally determined characteristics of microfluidics-prepared CUR-PNPs are listed in *Supporting Information* (Table S3) and described in the text.

Transmission Electron Microscopy. Negatively-stained samples for transmission electron microscopy (TEM) imaging were prepared by depositing a drop of CUR-PNP dispersion on a carbon-coated 300-mesh copper TEM grid followed by a drop of 1 wt % uranyl acetate aqueous solution as a negative staining agent. Excess liquid was immediately removed using lens paper, followed by drying of the remaining liquid under ambient conditions. Imaging was performed on a JEOL JEM-1400 transmission electron microscope, operating at an accelerating voltage of 65 kV and equipped with a Gatan Orius SC1000 CCD camera.

Dynamic Light Scattering. Effective hydrodynamic diameters and size distributions of CUR-PNPs were determined using dynamic light scattering (DLS). DLS measurements were carried out using a Brookhaven Instruments Zeta-Pals Analyzer equipped with a solid state Laser (660 nm) with a maximum power output of 35 mW. All DLS measurements of CUR-PNPs were performed in pure water and an experimental temperature of 25˚C and at a scattering angle of 90˚. For each CUR-PNP preparation, mean effective hydrodynamic sizes were determined from three measurements of the autocorrelation function using cumulent analysis. Reported mean effective hydrodynamic diameters for each condition of r and Q were determined by averaging values from triplicate preparations. Errors on mean effective hydrodynamic diameters were calculated from the standard deviation (sd) of values obtained from triplicate preparations: $error = \frac{sd}{\sqrt{3}}$.

CUR Encapsulation Efficiency Determination. Encapsulation efficiencies of CUR-PNPs were determined by high performance liquid chromatography (HPLC). Water was removed

from ~1 g of a gravimetrically determined quantity of PNP dispersion by rotary evaporation at 25 °C; then ~0.5 g of a gravimetrically determined quantity of acetonitrile was added to the resulting solid and the mixture was vortexed for 30 s to ensure complete dissolution of drug. HPLC (Ultimate 3000, Thermo Scientific) with a C18 column (Phenomenex Luna 5u C18), a constant eluent composition of 65/35 acetonitrile/water (v/v) with 0.3 v % acetic acid, and a diode array detector (DAD) set at 420 nm, was then used to quantify the concentration of drug in the resulting solutions. Sample injection volumes were 50 μL and the flow rate was 1 mL/min. A calibration curve for the DAD was generated by analysis of 6 standards containing different known CUR concentrations in acetonitrile. Quantities of CUR in the various dissolved CUR-PNP solutions were determined and encapsulation efficiencies (*EE*) and drug loadings (*DL*) were calculated for each sample using the following equations:

$$EE\ /\ \% = \frac{mass\ encapsulated\ CUR}{total\ mass\ CUR} \times 100$$

$$r = \frac{total\ mass\ CUR}{mass\ copolymer}$$

$$DL\ /\ \% = \frac{mass\ encapsulated\ CUR}{mass\ encapsulated\ CUR + mass\ copolymer} \times 100$$

$$DL\ /\ \% = \frac{r \times EE}{(r \times EE) + 1} \times 100$$

Reported *EE* and *DL* values for each condition of *r* and *Q* were determined by averaging values from triplicate preparations, with reported errors calculated from standard deviations across the triplicate preparations: $error = \frac{sd}{\sqrt{3}}$.

***In Vitro* CUR Release Kinetics.** Experiments were carried out to monitor the *in vitro* release of CUR from CUR-PNPs using HPLC. In a typical experiment, CUR-PNPs were divided

into 10 parts and each part was transferred to a 2 mL Float-A-Lyzer tube (SpectrumLabs, MWCO 6-8 kDa) for each predetermined time. For preliminary experiments comparing bulk and microfluidic PNPs, different Float-A-Lyzer tubes were used (SpectrumLabs, MWCO 100 kDa) were used. These tubes were then placed in a 5-L beaker of the release medium, consisting of ~2 L of PBS; throughout release experiments, the release medium was constantly stirred using magnetic stirring and maintained at physiological temperature (37 °C). At each predetermined time, the solution of a single tube was transferred to a vial and then dried by rotary evaporation at 25 °C. After that ~0.2 g of a gravimetrically determined quantity of acetonitrile was added. The resulting solution was injected into the HPLC and CUR was detected by DAD. Percentages of CUR released were calculated relative to the determined amount of CUR in PNPs at the t = 0 release time. Reported release percentages at each time are averages determined from triplicate preparations under the specified conditions, with reported errors calculated from standard deviations across the triplicate preparations: $error = \frac{sd}{\sqrt{3}}$.

Cell-Culture and Antiproliferation Assay. MDA-MB-231 cells were grown to ~80% confluence in Dulbecco's Modified Eagle's Medium (DMEM) supplemented with 10% fetal bovine serum (FBS) in a 75 cm^2 tissue culture flask and maintained at 37 °C with 5% CO_2 in a tissue culture incubator. Cells were then trypsinized, collected and pelleted by centrifugation at 4 ºC and 1200 rpm for 5 minutes. The cell pellet was then resuspended in DMEM media and the cell concentration was determined using a hemocytometer. After the initial cell concentration was determined the suspension was diluted to 1.0×10^5 cells/mL. Next, a multichannel pipet was used to fill a 96 well plate with 100 µL/ well of the diluted cell suspension. The cell loaded plates were then incubated for 24 h at 37 °C under an atmosphere of 5% CO_2.

After 24 hours cell incubation, 65 µL aliquots of stock CUR-PNP dispersions or 65 µL of free CUR dissolved in dimethylsulfoxide (DMSO) were diluted to a total volume of 650 µL with DMEM media. Serial dilutions were carried out, and then 100 µL of each diluted stock was added to the appropriate well of the 96-well plate (containing ~1.0×10^4 cells in 100 µL of media, as described above), in order to generate a range of different concentrations for analysis. The treated cells were incubated for 48, 72 or 96 hours at 37 °C under a 5% CO_2 atmosphere. In order to determine cell viability, 20 µL of CellTiter-Blue was added to each well after the predetermined incubation time was complete. After the addition of the CellTiter-Blue the 96 well plates were incubated for 4 hours (5% CO_2, 37 °C) and then fluorescence (λ_{ex} = 560 nm; λ_{em} = 590 nm emission) readings were recorded on a 96-well plate reader. Cell death was calculated for each well, based upon the following formula:

$$\%\, Death = \left[1 - \frac{(S - B_o)}{(B_t - B_o)}\right] \times 100$$

where S is the sample reading (cells + drug + media), B_t is the average reading for the untreated population of cells (cells + media), and B_0 is the average reading of wells containing media only (media). *% Death* vs. CUR concentration data sets, which combined data from three separate CUR-PNP preparations for each condition, were fit using XLfit (IDBS). Reported IC_{50} values were derived by combining all three data sets into a single curve and then calculating the overall concentration required to elicit a 50% reduction in cell viability. Errors on reported IC_{50} values were assessed using: $error = \frac{sd}{\sqrt{3}}$, plotting each data set individually, determining IC_{50} values for individual data sets, then calculating a standard deviation across the three measured values.

Results and Discussion

Encapsulation Efficiencies and Drug Loading Levels in CUR-PNPs

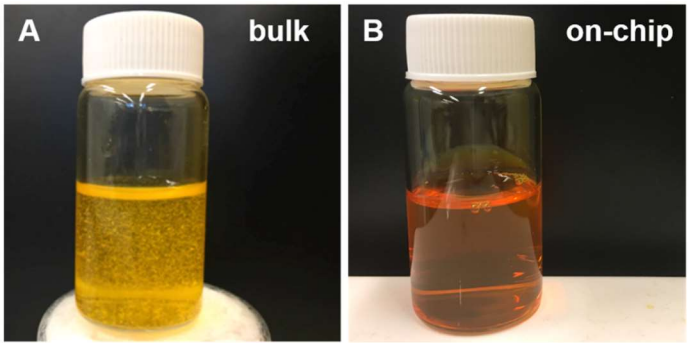

Figure 2. Photos of aqueous dispersions of CUR-PNPs with equal concentrations of CUR (0.25 mg/mL) and PCL-*b*-PEO (0.33 mg/mL) prepared by (A) conventional ("bulk") nanoprecipitation methed and (B) gas-liquid microfluidic reactor at a flow rate of Q = 200 µL/min.

CUR-PNP manufacturing on the gas-liquid microfluidic reactor resulted in greatly improved CUR encapsulation efficiency and drug loading levels compared to the conventional nanoprecipitation method ("bulk preparation"). Figure 2 compares photographs of aqueous CUR-PNP dispersions containing approximately equal concentrations of CUR (0.25 mg/mL) and PCL-*b*-PEO (0.33 mg/mL) prepared by the nanoprecipitation method (Figure 2A) and by the microfluidic method at a flow rate of Q = 200 µL/min (Figure 2B). Both photographs were taken after dialysis of CUR-PNPs but before centrifugation to remove unencapsulated drug. The bulk-prepared dispersion is a light yellow colour with a large amount of solid precipitate, indicating a relatively small amount of encapsulated CUR dispersed in water and a relatively large amount of insoluble, unencapsulated CUR (Figure 2A). On the other hand, the microfluidic-prepared dispersion is a dark yellow/orange colour with no visible precipitate, indicating a relatively large

amount of encapsulated CUR dispersed in water and a relatively small amount of insoluble, unencapsulated CUR (Figure 2B).

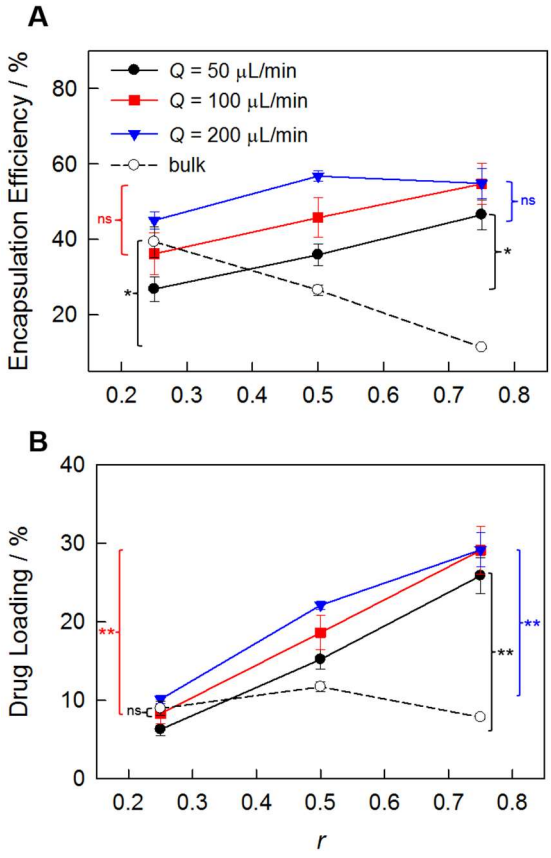

Figure 3. Plots of encapsulation efficiency (A) and drug loading (B) vs. CUR loading ratio, r for various preparations of CUR-PNPs using both bulk and microfluidic methods. Data for microfluidic preparations are plotted for three different manufacturing flow rates, Q = 50, 100, and 200 μL/min. Statistical comparisons of r = 0.25 and r = 0.75 data points are indicated with ** ($p < 0.005$), * ($p < 0.05$), or ns ($p > 0.05$).

Quantitative comparisons of encapsulation efficiencies (*EE*) and drug loading percentages (*DL*) for bulk and microfluidic preparations of CUR-PNPs are provided in Figure 3. For bulk preparations, Figure 3A shows a steady decrease in the encapsulation efficiency as the amount of added CUR increases (*EE* vs. *r*), corresponding to a relatively constant loading level (~10%) in Figure 3B (*DL* vs. *r*). Similar trends have been observed for other conventional preparations of

CUR-PNPs, and reflect a constant encapsulation capacity for CUR within the block copolymer core.[37, 53] As a result, the amount of encapsulated CUR stays constant as more CUR relative to polymer is added, resulting in the observed decrease in encapsulation efficiency. In contrast, we find that microfluidic preparations show a general increasing trend in both encapsulation efficiency (Figure 3A) and loading level (Figure 3B) as the amount of CUR relative to polymer in the formulation, *r*, increases. We carried out *t*-test comparisons between the first and last data points and found that for some flow rates the increase in *EE* between $r = 0.25$ and $r = 0.75$ was not statistically significant due to experimental error despite the consistent increasing trend (Figure 3A). However, the same statistical comparison yielded significant increases in *DL* with increasing *r* for all microfluidic preparations (Figure 3B).

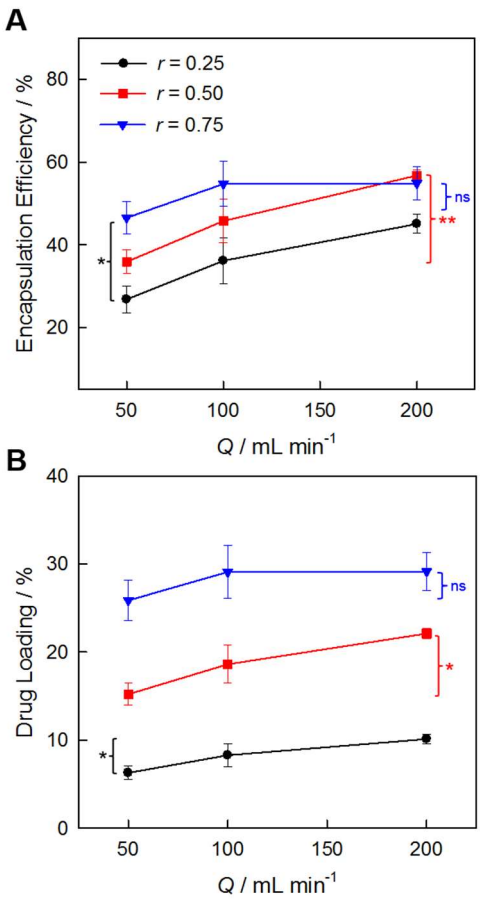

Figure 4. Plots of encapsulation efficiency (A) and drug loading (B) vs. manufacturing flow rate, *Q*, for microfluidic preparations of CUR-PNPs. Data are plotted for three different CUR loading ratios, r = 0.25, 0.50, and 0.75. Statistical comparisons of Q = 50 µL/min and Q = 200 µL/min data points are indicated with ** ($p < 0.005$), * ($p < 0.05$), or ns ($p > 0.05$).

For the microfluidic preparations, we also plot these data as *EE* vs. *Q* (Figure 4A) and *DL* vs. *Q* (Figure 4B) for each of the three loading ratios, r = 0.25 (black line), 0.50 (red line), and 0.75 (blue line). These plots show statistically significant increases in *EE* and *DL* as the manufacturing flow rate increases from Q = 50 µL/min and Q = 200 µL/min for the r = 0.25 and r = 0.50 loading ratios. For the r = 0.75 loading ratio, increasing trends in *EE* and *DL* with increasing *Q* are also found, although the increases are found to be not statistically significant due to larger error bars in that series. Within the range of *Q* and r values explored in the microfluidic

preparations summarized in Figures 3 and 4, we achieved a maximum drug loading of DL = 29 ± 5% for the r = 0.75, Q = 200 μL/min condition, which is, to our knowledge, the highest loading level achieved so far for CUR within block copolymer nanoparticles. Other studies have used microfluidic reactors to encapsulate CUR,[52, 70] although those employed single-phase reactors without high-shear effects.[65] An encapsulation efficiency of 96% (DL = 15%) was obtained by Guo et al. using a "T-junction" mixer,[52] while the Ozeki group used a "herringbone" reactor to achieve EE = 20-50% (DL = 2-5%).[70] It is important to note that the polymers used in those studies (a PCL-*b*-PEO-*b*-PCL triblock in ref. 52 and various PLGA-PEO copolymers in ref. 70) were different than the PCL-*b*-PEO copolymer employed here, and the loading ratios were lower than our range of r = 0.25-0.75 (r = 0.19 and r = 0.10, respectively). Therefore, it is impossible based on existing data to meaningfully compare EE values in these various types of microfluidic mixers.

The extraordinary increases in EE and DL with increasing r and Q in microfluidic preparations (Figures 3 and 4) are attributed to processing effects within variable high-shear "hot spots" of the microfluidic channels that are not present in bulk preparations. We have shown in previous work that encapsulation efficiency of PAX in PCL-*b*-PEO PNPs is negatively correlated with the crystallinity of the PCL core,[57] since molecular cargo tends to be excluded from low-enthalpy crystallites and preferentially solubilized in high-entropy amorphous regions. In the same study, we showed strong suppression of PCL core crystallinity (and a corresponding increase in encapsulation efficiency) as the loading ratio of added PAX increased in the range $r > 0.5$.[57] This suggests that non-polymeric additives can have a plasticizing effect on the semicrystalline PCL core by intercalating and disrupting chain order within crystallites. We speculate that in the current microfluidic preparations CUR also acts as a plasticizer such that the amorphous volume (hence the encapsulation capacity) increases as more CUR relative to polymer is added (Figure 3). Similar

positive trends in *EE* and *DL* with increasing *r* are not observed in the bulk preparations, suggesting a requirement of high shear for CUR-induced increases in encapsulation capacity.

The importance of shear processing for the microfluidic preparations is obviated by the increases in *EE* and *DL* with flow rate, *Q* (Figure 4), since the maximum shear rate within the "hot spots" increases linearly with *Q*. We note that in our previous studies of PAX encapsulation within the gas-liquid microfluidic reactor,[57,66] *EE* values either increased[66] or decreased[57] with increasing flow rate, depending on the initial loading ratio of drug. In those studies, increases in *EE* with increasing *Q* were attributed to shear-induced coalescence producing non-spherical morphologies with larger hydrophobic volumes,[66] whereas decreases in *EE* with increasing *Q* were attributed to shear-induced crystallization excluding drug from the core.[57] In the current case of CUR encapsulation, the observed increase in *EE* with increasing *Q* cannot be due to an increase in particle size, since PNP size is found to decrease with *Q* as discussed in the next section. One possible explanation, consistent with the increase in *EE* with *r* discussed above, is that an increasing shear rate with increasing *Q* facilitates better contact between CUR and the PCL blocks, leading to greater plasticization of PCL crystallites and consequentially a larger amorphous PCL volume for CUR encapsulation. This comparison with PAX encapsulation also highlights that shear processing effects within two-phase microfluidic reactors, while providing a useful handle on structure and properties in PNP drug delivery systems, can be strongly dependent on the specific chemical parameters of a given formulation.

CUR-PNP Morphologies and Size Distributions

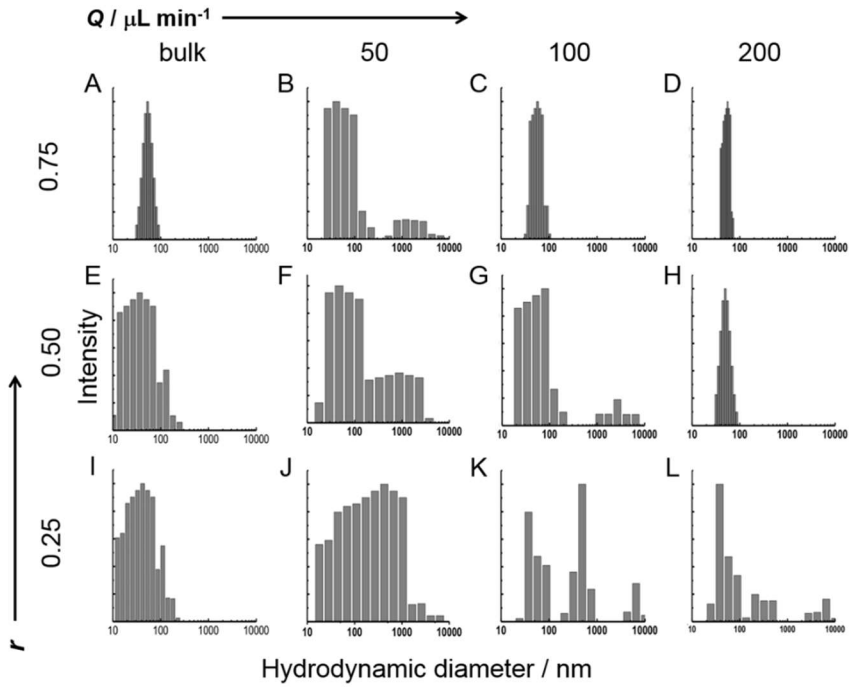

Figure 5. CONTIN size distributions from DLS data for various preparations of CUR-PNPs using both bulk (A, E, I) and microfluidic (B-D, F-H, J-L) methods.

DLS size distributions from CONTIN analysis of 12 different bulk- and microfluidic-prepared CUR-PNP samples from various formulation conditions are shown in Figure 5. The 12 samples represent three different CUR loading ratios (r = 0.25, 0.50, or 0.75) and four different bulk and microfluidic flow conditions (Q = 0 (bulk), 50, 100, and 200 μL/min). From the array of histograms, is clear that the presence of larger aggregates within the distribution (d_h > 100 nm) diminishes with increasing r (increasing added CUR relative to polymer) for all bulk and microfluidic preparations. Also, for all microfluidic preparations, CONTIN results suggest that size distributions become narrower with increasing flow rate, Q. This is also evidenced by DLS polydispersity indexes (PDI) for the r = 0.75 series, which decrease as flow rate increases from PDI = 0.25 ± 0.02 (Q = 50 μL/min) to 0.18 ± 0.01 (Q = 100 μL/min) to 0.12 ± 0.03 (Q = 200

μL/min). At the lowest microfluidic flow rate, Q = 50 μL/min, CONTIN distributions for each r value show a strong population centered below 100 nm along with one or more populations centered well above 100 nm (Figure 5, B, F and J). As the flow rate increases, the populations of larger particles diminish and then disappear, except in the r = 0.25 case where there are still residual contributions of larger particles even at Q = 200 μL/min (Figure 5L). In each of the r = 0.50 and 0.75 cases, the Q = 200 μL/min flow rate results in a single narrow distribution of particles centered below 100 nm (Figure 5, D and H).

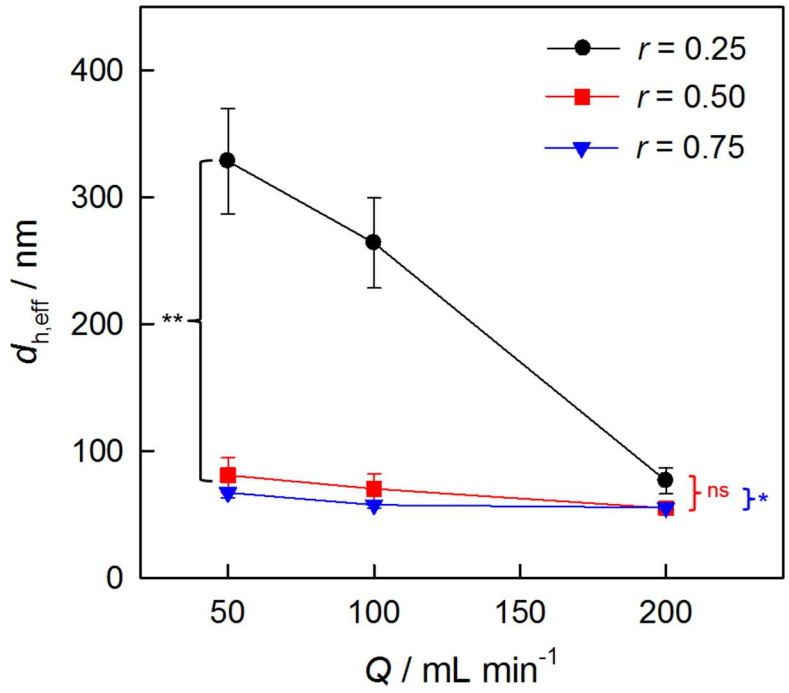

Figure 6. Plots of effective hydrodynamic diameters, $d_{h,eff}$, vs. manufacturing flow rate, Q, from cumulant analysis of DLS data for microfluidic preparations of CUR-PNPs. Data are plotted for three different CUR loading ratios, r = 0.25, 0.50, and 0.75. Statistical comparisons of Q = 50 μL/min and Q = 200 μL/min data points are indicated with ** ($p < 0.005$), * ($p < 0.05$), or ns ($p > 0.05$).

For each of the microfluidic preparations, Figure 6 shows plots of mean effective hydrodynamic diameter ($d_{h,eff}$), determined from cumulent analysis of DLS data, vs. flow rate, Q. Consistent with the particle size distributions in Figure 5, Figure 6 shows a general trend of decreasing $d_{h,eff}$ as the manufacturing flow rate increases for all three loading ratios. The extent of flow-induced size reduction is greatest for the lowest loading ratio, $r = 0.25$ (black line), where mean $d_{h,eff}$ values decrease from 328 ± 72 nm for $Q = 50$ µL/min to 76 ± 18 nm for $Q = 200$ µL/min (statistically significant decrease, $p < 0.005$). This marked decrease in mean size is consistent with the strong contribution from large particle populations ($d_h >> 100$ nm) at the $r = 0.25$ loading ratio, which significantly decreases as flow rate increases (Figure 5, J-L). For the intermediate and high loading ratios, $r = 0.50$ (red line) and $r = 0.75$ (blue line), the same increase in flow rate results in decreases in $d_{h,eff}$ from 81 ± 24 nm to 55 ± 3 nm (statistically significant decrease, $p < 0.05$) and from 67 ± 7 nm to 55 ± 2 nm (no significant difference, $p > 0.05$), respectively. These less dramatic decreases in mean size are also consistent with the diminishment of large particle populations with increasing flow rate observed in the corresponding size distributions (Figure 5).

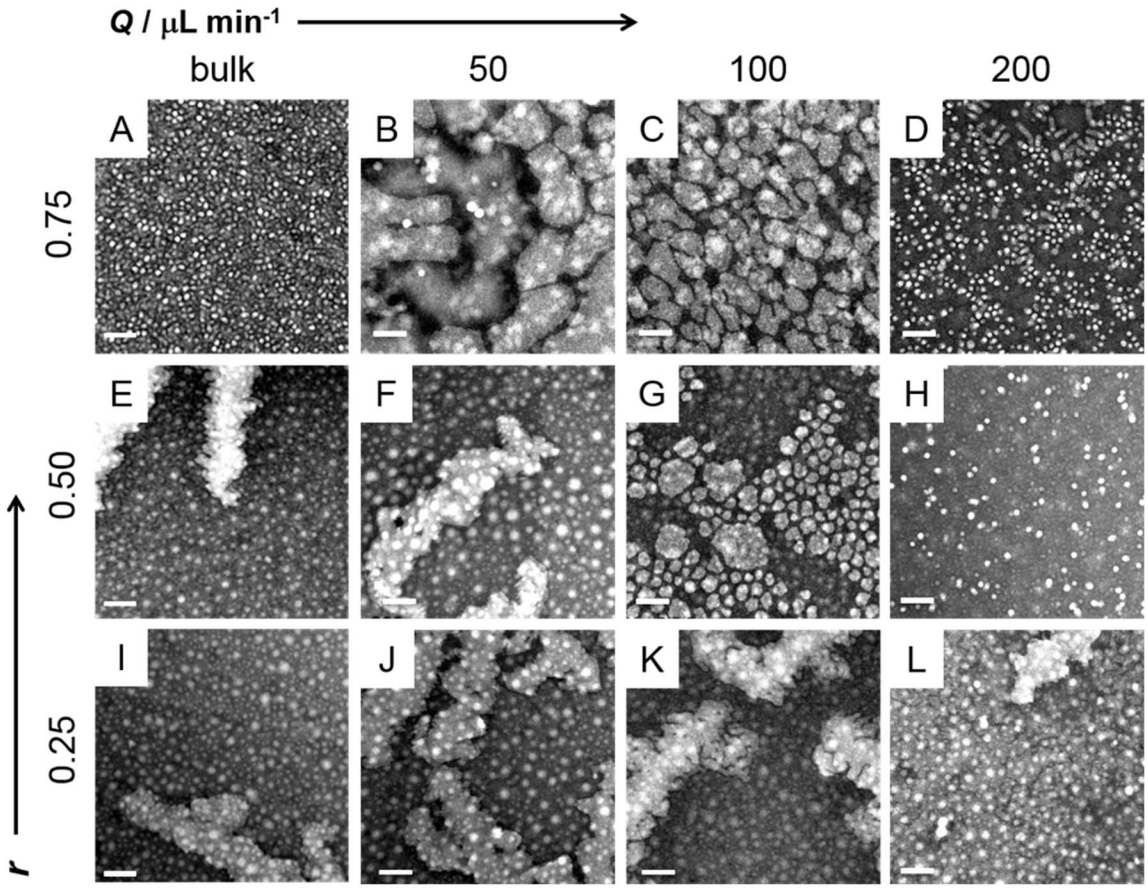

Figure 7. TEM images for various preparations of CUR-PNPs using both bulk (A, E, I) and microfluidic (B-D, F-H, J-L) methods. All scale bars are 200 nm.

Figure 7 shows TEM images of the 12 CUR-PNPs preparation conditions represented by the DLS size distributions in Figure 5. The TEM images are generally in good agreement with the DLS size distributions, showing a combination of small spheres and large, irregular-shaped aggregates, resembling lamellae or continents, under most conditions of *r* and *Q*. Consistent with the DLS histograms, for microfluidic preparations the continents are largest and most numerous at the lowest flow rate (Q = 50 μL/min), and decrease in size and number as the flow rate increases. For the r = 0.50 and 0.75 loading ratios, increasing the flow rate eventually leads to a single population of small (d = ~40 nm), low-polydispersity spheres at Q = 200 μL/min (Figure 7, D and

H). This TEM sphere size corresponds to the PCL cores and is therefore quite consistent with the corresponding mean hydrodynamic diameter from DLS ($d_{h,eff}$ = 55 nm), which includes the contribution of solubilized PEO chains.

The observed effect of CUR loading ratios on size distributions (Figure 5) and mean particle sizes (Figure 6) for both bulk and microfluidic preparations is explained by the role of CUR as a plasticizer of the PCL blocks in PNP cores. Large, low-curvature aggregates such as lamellae are favoured by high degrees of core chain crystallization.[71] Therefore, the extent of large aggregate formation is reduced by the addition of more CUR, which suppresses PCL crystallization and favours small, high-curvature spheres. As a result, mean particle sizes are significantly larger for the lowest CUR loading ratio, r = 0.25, due to greater contributions from large aggregates. The greater contribution of PCL crystallization also explains the higher error bars on mean particle sizes in the r = 0.25 series (Figure 6), since time-dependent crystallization-driven growth will lead to stronger kinetic contributions and lower reproducibility of particle sizes.[71] This effect is one example of the general sensitivity of PNP sizes, size distributions, and morphologies to CUR loading ratios, as has been found in other studies.[37, 40, 43, 47, 53]

A key feature of the two-phase gas-liquid microfluidic reactor employed here is the application of polymer shear processing *via* variable flow rate in the microfluidic channel, as demonstrated by the strong effect of flow rate Q on particle size distributions (Figure 5), mean particle sizes (Figure 6), and morphologies (Figure 7). For example, in the microfluidic reactor, both DLS distributions (Figure 5) and TEM images (Figure 7) show that the relative contributions of large aggregates and small spheres to CUR-PNP populations can be varied with flow rate for all three CUR loading ratios. Specifically, the large aggregate contributions decrease with increasing flow rate, attributed to an increase in shear-induced particle break-up of large

aggregates as the maximum shear rate in the "hot spots" increases.[60,62] In fact, at the highest flow rate (Q = 200 μL/min), the large aggregates disappear completely, except in the r = 0.25 case, due to greater contributions of large aggregates at the lowest CUR loading ratio as discussed above. These high-shear "hot spots" are unique to two-phase microfluidic systems, enabling flow-variable tuning of particle size distributions, independent of the chemical conditions. In a previous study, we showed that a commercial single-phase herringbone microfluidic reactor, while acting as a fast and efficient mixer to trigger PNP self-assembly, does not provide sufficiently high shear to enable processing control of PNP sizes and morphologies.[65] In fact, a similar herringbone reactor was recently used to produce CUR-loaded PLGA PNPs, resulting in only very modest changes in PNP diameter between ~225 nm and ~175 nm as the total flow rate increased.[70] The flow-dependent PNP sizes in ref. 70 are not well understood, but may be attributed to differences in PLGA nucleation and growth; they are not associated with high shear processing due to the absence of sufficiently high shear in the single-phase herringbone reactor.[65] We believe that the current two-phase microfluidic system provides significantly greater control and flexibility, based on high-shear PNP processing, for CUR-PNP formulation optimization than other microfluidic or bulk manufacturing methods. Based on their relatively high loading efficiencies and generally smaller particle sizes, we chose CUR-PNP formulations prepared with a loading ratio of r = 0.75 for subsequent experiments on the effects of microfluidic processing on CUR release rates and MDA-MB-231 cytotoxicity assays.

Flow-Variable CUR Release Profiles from CUR-PNPs

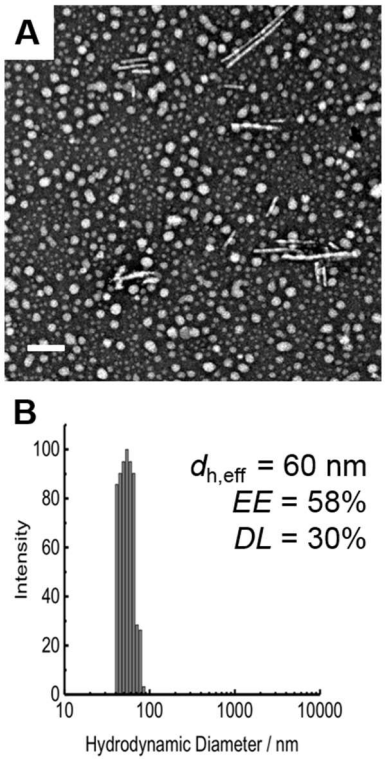

Figure 8. (A) TEM image and (B) CONTIN size distribution from DLS data for CUR-PNPs prepared at a CUR loading ratio of r = 0.75 in the microfluidic reactor at a manufacturing flow rate of Q = 400 μL/min. The inset to (B) lists the effective hydrodynamic diameter, $d_{h,eff}$, from cumulant analysis of DLS data, along with encapsulation efficiency (*EE*) and drug loading (*DL*) values for the sample. The scale bar is 200 nm.

The microfluidic CUR-PNP sample prepared with a loading ratio of r = 0.75 and a flow rate of Q = 200 μL/min was selected for CUR release experiments based on its high drug loading level (*DL* = 29%) and relatively small ($d_{h,eff}$ = 55 nm), low-polydispersity spheres. Preliminary experiments found that CUR-PNPs prepared in the bulk and in the microfluidic reactor at Q = 200 μL/min gave similar release profiles (*Supporting Information*, Figure S1). However, to determine the effect of microfluidic flow rate on CUR release, we prepared a sample at the same loading ratio using an even higher flow rate of Q = 400 μL/min. Characterization of the resulting Q = 400

μL/min sample (Figure 8) revealed a similar high CUR loading level (*DL* = 30%) and a similarly narrow distribution of small spheres ($d_{h,eff}$ = 60 nm) compared to the *Q* = 200 μL/min preparation. The slightly larger DLS particle size in the *Q* = 400 μL/min sample may be due to the presence of a small number of long, filament-shaped aggregates detected in the TEM images (Figure 8A), attributed to shear-induced coalescence of small particles,[60] that are not observed in TEM images of CUR-PNPs prepared at *Q* = 200 μL/min (Figure 7D).

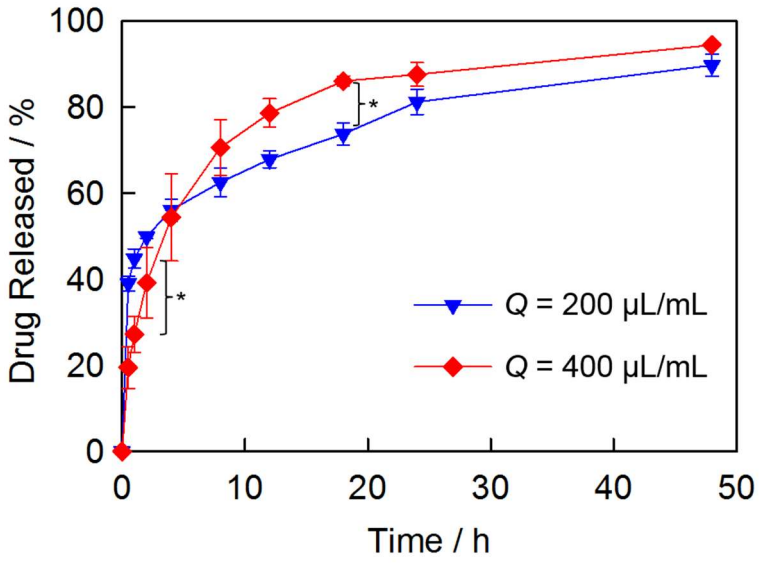

Figure 9. *In vitro* CUR release profiles for CUR-PNPs prepared in the microfluidic reactor at two different manufacturing flow rates, *Q*. Labeled statistical comparisons (*) indicate significant difference between curves at *t* = 1 h ($p = p < 0.05$) and *t* = 18 h ($p < 0.05$).

The *in vitro* CUR release profiles provide a baseline for future *in vivo* testing as they could affect pharmacokinetics and drug concentrations at the tumour site.[67] Figure 9 shows the release profiles of CUR-PNPs prepared at microfluidic flow rates of *Q* = 200 μL/min (blue line) and *Q* = 400 μL/min (red line). Both cases show extended CUR release over *t* > 48 h but with significantly different release kinetics in both fast and slow regions of the curves, as shown by *t*-test comparisons ($p < 0.05$) of release percentage values at *t* = 1 h and *t* = 18 h time points in Figure 9.

The Q = 200 μL/min sample shows faster initial CUR release reaching 40% released CUR in 30 min, compared to 2 h for the Q = 400 μL/min sample. This indicates significant suppression of "burst" release for CUR-PNPs formed at the higher flow rate. After 40%, CUR release from the Q = 200 μL/min sample slows down abruptly compared to a more gradual decline in release rate from the Q = 400 μL/min sample. After 48 h, 90% and 94% of CUR was released from the Q = 200 μL/min and Q = 400 μL/min samples, respectively, with no further release after 72 h in both cases. The significant difference in the release profiles is further demonstrated by differences in their respective fitted functions, with the Q = 400 μL/min profile fitting well to a 3-parameter hyperbolic model (*Supporting Information*, Figure S2). Using the same function, we were unable to obtain a good fit to the Q = 200 μL/min release data, which instead was fit using a 4-parameter hyperbolic model (*Supporting Information*, Figure S2).

The flow rate-dependent differences in the release profiles for CUR-PNPs of similar sizes and loading levels (Figure 9) indicates that microfluidic shear processing provides an experimental handle on CUR release kinetics that is independent of other important figures of merit for CUR delivery, including CUR-PNP size and loading amount. This suggests that flow rate could provide a useful handle on the pharmacokinetics of microfluidic CUR-PNP formulations without adversely affecting size-dependent EPR effects. In previous work, we have shown that paclitaxel-loaded PNPs prepared in the microfluidic channels showed decreased rates of drug release as the manufacturing flow rate increased,[27, 57, 66] which was attributed to shear-induced crystallization[57, 66] or to mixing-related differences in the drug distribution within the cores.[27] The current results show more complex effects of flow rate on the drug release kinetics, with increased flow rate triggering a combination of slower short-time and faster long-time regions within the release profile. Although these effects are not fully understood, they may be related to shear-induced

changes in the partitioning of CUR among the various microregions within the CUR-PNPs, including the amorphous core domains, crystalline core domains, corona, and core-corona interface, with different convolutions of release rates from these different regions leading to differences in the overall release profiles.

In Vitro CUR-PNP Cytotoxicity

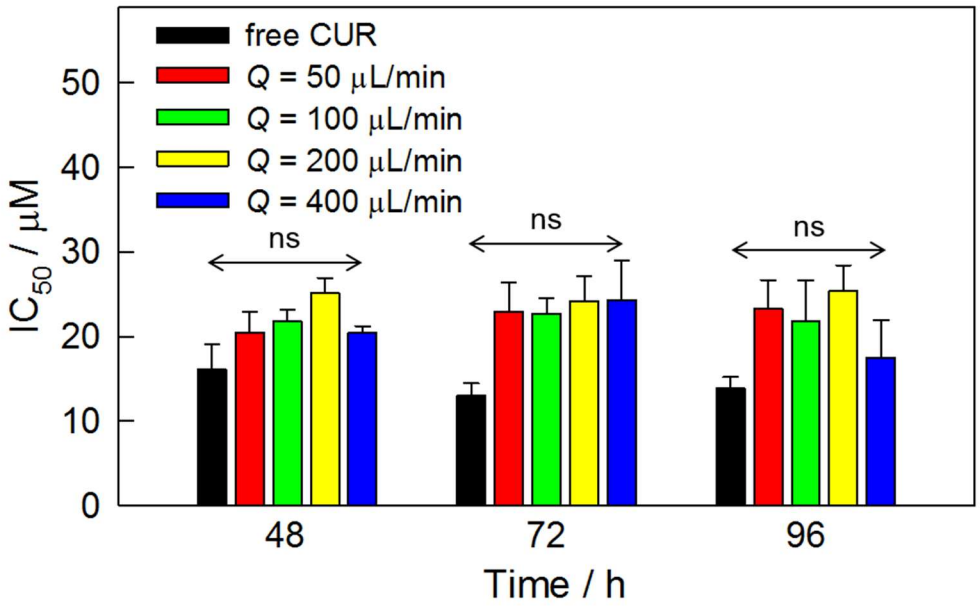

Figure 10. Potency against MDA-MB-231 breast cancer cells. Chart shows IC_{50} values for free CUR and CUR-PNPs ($r = 0.75$) prepared in the microfluidic reactor at four different manufacturing flow rates. Data is shown for incubation times of 48 h, 72 h, and 96 h. Labeled statistical comparisons (*) indicate no significant difference ($p > 0.05$) between free drug and PNP formulations, as well as no significant difference between PNPs prepared at different flow rates.

The series of microfluidic CUR-PNPs prepared with a loading ratio of $r = 0.75$ at four different flow rates (Q = 50, 100, 200, and 400 μL/min) were next tested for cytotoxic effects against the MDA-MB-231 breast cancer cell line. Free CUR was evaluated as a positive control

and empty PNPs without CUR were evaluated as a negative control. For all CUR-PNP samples and positive controls, cell death plots were generated for 48 h, 72 h, and 96 h incubation times (*Supporting Information*, Figures S3 and S4). Negative controls show no significant effect of the empty micelles on cell viability, with negligible cell death by empty PNPs measured up to a polymer concentration of 830 ppm (*Supporting Information*, Figure S5), which was higher than the highest polymer concentration applied in doses of CUR-PNPs (660 ppm).

IC_{50} values determined for 48 h, 72 h, and 96 h incubation times (Figure 10) were in the micromolar range, typical of CUR formulations.[36] Although for each incubation time we consistently find lower IC_{50} values for the free drug compared to the various CUR-PNP formuations, these differences were not found to be statistically significant. This is in contrast to previous results showing decreased PNP cytotoxicities compared to the free drug in PAX[27,57] and CUR[38,42,44] formulations and indicates that already low potencies of free CUR are not significantly attenuated by this microfluidic encapsulation method. Importantly, we find that microfluidic CUR-PNP formulations prepared at different flow rates do not show statistically different cytotoxicity effects. This is an intriguing result, since our previous work on PNP encapsulation of PAX using an identical gas-liquid microfluidic reactor showed antiproliferation effects against MCF-7 cells to be significantly dependent on manufacturing flow rate.[27, 57] We point out that in the current system flow-variable shear processing within the microchannels enables changes in size and size-distributions (Figures 5-7) and changes in release rates (Figure 9) without significantly affecting the IC_{50} values (Figure 10). Looking ahead to future *in vivo* studies, we expect that the ability to systematically vary biodistributions (*via* size) and pharmacokinetics (*via* release rates) while maintaining constant cytotoxicity will provide a unique processing handle for optimizing CUR delivery systems. We finally note that there is no clear trend in IC_{50} values with incubation time.

For the 48 h, 72 h, and 96 h incubation times, we obtain mean IC_{50} values for the CUR-PNP formulations (averaged over all microfluidic flow rates) of 22, 24, and 22 μM. A similar absence of time dependence for CUR IC_{50} values against MCF-7 has been previously observed.[47] The present result is not particularly surprising, considering the function of CUR as a relatively weak and nonspecific cytotoxic agent acting simultaneously on multiple cellular processes on a wide range of time scales.

Conclusions

Using a two-phase gas-liquid microfluidic reactor we have demonstrated shear processing control of the structure and properties of PCL-*b*-PEO PNPs with CUR encapsulated within CUR-PNPs. CUR-PNPs prepared by conventional nanoprecipitation show decreased encapsulation efficiency and constant drug loading as the CUR to copolymer ratio increases. In contrast, CUR-PNPs prepared by microfluidic manufacturing show encapsulation efficiencies and drug loading that both increase as the CUR to copolymer ratio increases, allowing drug loadings of up to 30 % (mass encapsulated CUR / mass CUR-PNPs) to be achieved. We have also shown that microfluidic shear processing provides a flow-directed handle on CUR-PNP size distributions without changing the chemical conditions, with increasing manufacturing flow rate leading to decreased mean CUR-PNP sizes and polydispersities within the EPR regime (~50 nm). Moreover, shear processing in the microfluidic channels enables CUR release profiles to be tuned under constant chemical conditions, with increased flow rate producing CUR-PNPs with suppressed "burst release" (slower initial and faster extended release). Finally, we compare *in vitro* effects of free CUR and CUR-PNPs prepared at various flow rates against MDA-MB-231 cancer cells, and find no significant attenuation in cytotoxicity for CUR-PNPs compared to free CUR and no significant effect of flow rate on IC_{50} values of microfluidic-prepared CUR-PNPs. The jury is still out on whether the poor

pharmacokinetics and efficacies of curcumin, along with its status as a pan-assay interference compound,[34] can be overcome by strategic formulation, in order to meet its vast expectations as a therapeutic "magical molecule".[36] However, within the context of that broader discussion, the current results highlight the unique capabilities of microfluidic shear processing for producing copolymer-based CUR nanomedicines of controlled structure and properties. They also suggest strong potential of this microfluidic platform for flow-directed optimization of CUR formulations toward improved medical outcomes.

Supporting Information. Additional release data and fits for bulk and microfluidic prepared CUR-PNPs; complete MDA-MB-231 cytotoxicity data for CUR and CUR-PNPs; percentage cell death for empty (control) PNPs; tables of CUR-PNP characteristics; table of actual flow rates

Acknowledgements. We are grateful to the Natural Sciences and Engineering Research Council of Canada, NSERC, for financial support. We acknowledge Dr. Patrick Nahirney and the UVic EM lab (Department of Biology) for the continued use of their TEM.

References

1. von Roemeling, C.; Jiang, W.; Chan, C. K.; Weissman, I. L.; Kim, B. Y., Breaking down the barriers to precision cancer nanomedicine. *Trends Biotechnol.* **2017,** *35*, 159-171.

2. Allen, C.; Maysinger, D.; Eisenberg, A., Nano-engineering block copolymer aggregates for drug delivery. *Colloids Surf. B* **1999,** *16*, 3-27.

3. Discher, D. E.; Ortiz, V.; Srinivas, G.; Klein, M. L.; Kim, Y.; Christian, D.; Cai, S.; Photos, P.; Ahmed, F., Emerging Applications of Polymersomes in Delivery: from Molecular Dynamics to Shrinkage of Tumors. *Prog. Polym. Sci.* **2007,** *32*, 838-857.

4. Branco, M. C.; Schneider, J. P., Self-assembling materials for therapeutic delivery. *Acta Biomater.* **2009,** *5*, 817-31.

5. Tyrrell, Z. L.; Shen, Y. Q.; Radosz, M., Fabrication of micellar nanoparticles for drug delivery through the self-assembly of block copolymers. *Prog. Polym. Sci.* **2010,** *35*, 1128-1143.

6. Gong, J.; Chen, M. W.; Zheng, Y.; Wang, S. P.; Wang, Y. T., Polymeric micelles drug delivery system in oncology. *J. Control. Release* **2012,** *159*, 312-323.

7. Kataoka, K.; Harada, A.; Nagasaki, Y., Block copolymer micelles for drug delivery: Design, characterization and biological significance. *Adv. Drug Deliver. Rev.* **2012,** *64*, 37-48.

8. Parveen, S.; Misra, R.; Sahoo, S. K., Nanoparticles: a boon to drug delivery, therapeutics, diagnostics and imaging. *Nanomed.-Nanotechnol.* **2012,** *8*, 147-166.

9. Lee, J. S.; Feijen, J., Polymersomes for drug delivery: Design, formation and characterization. *J. Control. Release* **2012,** *161*, 473-483.

10. Kwon, G. S.; Kataoka, K., Block copolymer micelles as long-circulating drug vehicles. *Adv. Drug Deliver. Rev.* **2012,** *64*, 237-245.

11. Rosler, A.; Vandermeulen, G. W. M.; Klok, H. A., Advanced drug delivery devices via self-assembly of amphiphilic block copolymers. *Adv. Drug. Deliver. Rev.* **2012,** *64*, 270-279.

12. Elsabahy, M.; Wooley, K. L., Design of polymeric nanoparticles for biomedical delivery applications. *Chem. Soc. Rev.* **2012,** *41*, 2545-2561.

13. Zhang, Y.; Chan, H. F.; Leong, K. W., Advanced materials and processing for drug delivery: The past and the future. *Adv. Drug Deliver. Rev.* **2013,** *65*, 104-120.

14. Nicolas, J.; Mura, S.; Brambilla, D.; Mackiewicz, N.; Couvreur, P., Design, functionalization strategies and biomedical applications of targeted biodegradable/biocompatible polymer-based nanocarriers for drug delivery. *Chem. Soc. Rev.* **2013,** *42*, 1147-1235.

15. Lu, Y.; Park, K., Polymeric micelles and alternative nanonized delivery vehicles for poorly soluble drugs. *Int. J. Pharm* **2013,** *453*, 198-214.

16. Ahmad, Z.; Shah, A.; Siddiq, M.; Kraatz, H. B., Polymeric micelles as drug delivery vehicles. *RSC Adv.* **2014,** *4*, 17028-17038.

17. Oltra, N. S.; Nair, P.; Discher, D. E., From Stealthy Polymersomes and Filomicelles to "Self" Peptide-Nanoparticles for Cancer Therapy. *Annu. Rev. Chem. Biomol.* **2014,** *5*, 281-299.

18. Sun, T.; Zhang, Y. S.; Pang, B.; Hyun, D. C.; Yang, M.; Xia, Y., Engineered nanoparticles for drug delivery in cancer therapy. *Angew. Chem. Int. Ed.* **2014,** *53*, 12320-12364.

19. Yokoyama, M., Polymeric micelles as drug carriers: their lights and shadows. *J. Drug Target.* **2014,** *22*, 576-583.

20. Prabhu, R. H.; Patravale, V. B.; Joshi, M. D., Polymeric nanoparticles for targeted treatment in oncology: current insights. *Int. J. Nanomed.* **2015,** *10*, 1001-1018.

21. Ulbrich, K.; Hola, K.; Subr, V.; Bakandritsos, A.; Tucek, J.; Zboril, R., Targeted Drug Delivery with Polymers and Magnetic Nanoparticles: Covalent and Noncovalent Approaches, Release Control, and Clinical Studies. *Chem. Rev.* **2016,** *116*, 5338-5431.

22. Park, E. K.; Kim, S. Y.; Lee, S. B.; Lee, Y. M., Folate-conjugated methoxy poly(ethylene glycol)/poly(epsilon-caprolactone) amphiphilic block copolymeric micelles for tumor-targeted drug delivery. *J. Control. Release* **2005,** *109*, 158-168.

23. Blanco, E.; Shen, H.; Ferrari, M., Principles of nanoparticle design for overcoming biological barriers to drug delivery. *Nat. Biotechnol.* **2015,** *33*, 941-951.

24. Hillmyer, M. A.; Tolman, W. B., Aliphatic Polyester Block Polymers: Renewable, Degradable, and Sustainable. *Acc. Chem. Res.* **2014,** *47*, 2390-2396.

25. Locatelli, E.; Franchini, M. C., Biodegradable PLGA-b-PEG polymeric nanoparticles: synthesis, properties, and nanomedical applications as drug delivery system. *J. Nanopart. Res.* **2012,** *14*.

26. Ahmed, F.; Discher, D. E., Self-porating polymersomes of PEG-PLA and PEG-PCL: hydrolysis-triggered controlled release vesicles. *J. Control. Release* **2004,** *96*, 37-53.

27. Xu, Z.; Lu, C.; Lindenberger, C.; Cao, Y.; Wulff, J. E.; Moffitt, M. G., Synthesis, Self-Assembly, and Drug Delivery Characteristics of Poly (methyl caprolactone-co-caprolactone)-b-poly (ethylene oxide) Copolymers with Variable Compositions of Hydrophobic Blocks: Combining Chemistry and Microfluidic Processing for Polymeric Nanomedicines. *ACS Omega* **2017,** *2*, 5289-5303.

28. Bodratti, A. M.; Alexandridis, P., Formulation of Poloxamers for Drug Delivery. *J. Funct. Biomater.* **2018,** *9*, 11.

29. Salem, M.; Rohani, S.; Gillies, E. R., Curcumin, a promising anti-cancer therapeutic: a review of its chemical properties, bioactivity and approaches to cancer cell delivery. *RSC Adv.* **2014,** *4*, 10815-10829.

30. Mahmood, K.; Zia, K. M.; Zuber, M.; Salman, M.; Anjum, M. N., Recent developments in curcumin and curcumin based polymeric materials for biomedical applications: a review. *Int. J. Biol. Macromol.* **2015,** *81*, 877-890.

31. Naksuriya, O.; Okonogi, S.; Schiffelers, R. M.; Hennink, W. E., Curcumin nanoformulations: a review of pharmaceutical properties and preclinical studies and clinical data related to cancer treatment. *Biomater.* **2014,** *35*, 3365-3383.

32. Shanmugam, M. K.; Rane, G.; Kanchi, M. M.; Arfuso, F.; Chinnathambi, A.; Zayed, M.; Alharbi, S. A.; Tan, B. K.; Kumar, A. P.; Sethi, G., The multifaceted role of curcumin in cancer prevention and treatment. *Molecules* **2015,** *20*, 2728-2769.

33. Devassy, J. G.; Nwachukwu, I. D.; Jones, P. J., Curcumin and cancer: barriers to obtaining a health claim. *Nutr. Rev.* **2015,** *73*, 155-165.

34. Nelson, K. M.; Dahlin, J. L.; Bisson, J.; Graham, J.; Pauli, G. F.; Walters, M. A., The essential medicinal chemistry of curcumin: miniperspective. *J. Med. Chem.* **2017,** *60*, 1620-1637.

35. Khandelwal, P.; Alam, A.; Choksi, A.; Chattopadhyay, S.; Poddar, P., Retention of Anticancer Activity of Curcumin after Conjugation with Fluorescent Gold Quantum Clusters: An in Vitro and in Vivo Xenograft Study. *ACS Omega* **2018,** *3*, 4776-4785.

36. Mehanny, M.; Hathout, R. M.; Geneidi, A. S.; Mansour, S., Exploring the use of nanocarrier systems to deliver the magical molecule; curcumin and its derivatives. *J. Control. Release* **2016,** *225*, 1-30.

37. Ma, Z.; Haddadi, A.; Molavi, O.; Lavasanifar, A.; Lai, R.; Samuel, J., Micelles of poly (ethylene oxide)-b-poly (ε-caprolactone) as vehicles for the solubilization, stabilization, and controlled delivery of curcumin. *J. Biomed. Mater. Res. A* **2008,** *86*, 300-310.

38. Song, L.; Shen, Y.; Hou, J.; Lei, L.; Guo, S.; Qian, C., Polymeric micelles for parenteral delivery of curcumin: preparation, characterization and in vitro evaluation. *Colloids Surf. A* **2011,** *390*, 25-32.

39. Feng, R.; Song, Z.; Zhai, G., Preparation and in vivo pharmacokinetics of curcumin-loaded PCL-PEG-PCL triblock copolymeric nanoparticles. *Int. J. Nanomed.* **2012,** *7*, 4089.

40. Yang, R.; Zhang, S.; Kong, D.; Gao, X.; Zhao, Y.; Wang, Z., Biodegradable polymer-curcumin conjugate micelles enhance the loading and delivery of low-potency curcumin. *Pharm. Res.* **2012,** *29*, 3512-3525.

41. Feng, R.; Zhu, W.; Song, Z.; Zhao, L.; Zhai, G., Novel star-type methoxy-poly (ethylene glycol)(PEG)–poly (ε-caprolactone)(PCL) copolymeric nanoparticles for controlled release of curcumin. *J. Nanopart. Res.* **2013,** *15*, 1748.

42. Song, Z.; Zhu, W.; Liu, N.; Yang, F.; Feng, R., Linolenic acid-modified PEG-PCL micelles for curcumin delivery. *Int. J. Pharm* **2014,** *471*, 312-321.

43. Raveendran, R.; Bhuvaneshwar, G.; Sharma, C. P., In vitro cytotoxicity and cellular uptake of curcumin-loaded Pluronic/Polycaprolactone micelles in colorectal adenocarcinoma cells. *J. Biomater. Appl.* **2013,** *27*, 811-827.

44. Zhu, W.; Song, Z.; Wei, P.; Meng, N.; Teng, F.; Yang, F.; Liu, N.; Feng, R., Y-shaped biotin-conjugated poly (ethylene glycol)–poly (epsilon-caprolactone) copolymer for the targeted delivery of curcumin. *J. Colloid Interf. Sci.* **2015,** *443*, 1-7.

45. Kumari, P.; Swami, M. O.; Nadipalli, S. K.; Myneni, S.; Ghosh, B.; Biswas, S., Curcumin delivery by poly (Lactide)-based co-polymeric micelles: an in vitro anticancer study. *Pharm Res.* **2016,** *33*, 826-841.

46. Gorinova, C.; Aluani, D.; Yordanov, Y.; Kondeva-Burdina, M.; Tzankova, V.; Popova, C.; Yoncheva, K., In vitro evaluation of antioxidant and neuroprotective effects of curcumin loaded in Pluronic micelles. *Biotechnol. Biotechnol. Equip.* **2016,** *30*, 991-997.

47. Manjili, H. K.; Ghasemi, P.; Malvandi, H.; Mousavi, M. S.; Attari, E.; Danafar, H., Pharmacokinetics and in vivo delivery of curcumin by copolymeric mPEG-PCL micelles. *Eur. J. Pharm. Biopharm.* **2017,** *116*, 17-30.

48. Tima, S.; Anuchapreeda, S.; Ampasavate, C.; Berkland, C.; Okonogi, S., Stable curcumin-loaded polymeric micellar formulation for enhancing cellular uptake and cytotoxicity to FLT3 overexpressing EoL-1 leukemic cells. *Eur. J. Pharm. Biopharm.* **2017,** *114*, 57-68.

49. Feng, R.; Deng, P.; Song, Z.; Chu, W.; Zhu, W.; Teng, F.; Zhou, F., Glycyrrhetinic acid-modified PEG-PCL copolymeric micelles for the delivery of curcumin. *React. Funct. Polym.* **2017,** *111*, 30-37.

50. Dutta, B.; Barick, K.; Verma, G.; Aswal, V.; Freilich, I.; Danino, D.; Singh, B.; Priyadarsini, K.; Hassan, P., PEG coated vesicles from mixtures of Pluronic P123 and l-α-phosphatidylcholine: structure, rheology and curcumin encapsulation. *Phys. Chem. Chem. Phys.* **2017,** *19*, 26821-26832.

51. Gong, F.; Chen, D.; Teng, X.; Ge, J.; Ning, X.; Shen, Y.-l.; Li, J.; Wang, S., Curcumin-Loaded Blood-Stable Polymeric Micelles for Enhancing Therapeutic Effect on Erythroleukemia. *Mol. Pharm.* **2017,** *14*, 2585-2594.

52. Guo, F.; Guo, D.; Zhang, W.; Yan, Q.; Yang, Y.; Hong, W.; Yang, G., Preparation of curcumin-loaded PCL-PEG-PCL triblock copolymeric nanoparticles by a microchannel technology. *Eur. J. Pharm Sci.* **2017,** *99*, 328-336.

53. Danafar, H., Study of the composition of polycaprolactone/poly (ethylene glycol)/polycaprolactone copolymer and drug-to-polymer ratio on drug loading efficiency of curcumin to nanoparticles. *Jundishapur J. Nat. Pharm. Prod.* **2017,** *12*.

54. Tong, F.; Chai, R.; Jiang, H.; Dong, B., In vitro/vivo drug release and anti-diabetic cardiomyopathy properties of curcumin/PBLG-PEG-PBLG nanoparticles. *Int. J. Nanomed.* **2018,** *13*, 1945.

55. Novelli, F.; De Santis, S.; Diociaiuti, M.; Giordano, C.; Morosetti, S.; Punzi, P.; Sciubba, F.; Viali, V.; Masci, G.; Scipioni, A., Curcumin loaded nanocarriers obtained by self-assembly of a linear d, l-octapeptide-poly (ethylene glycol) conjugate. *Eur. Polym. J.* **2018,** *98*, 28-38.

56. Bawn, C., Encyclopedia of polymer science and engineering: JI Kroschwitz, HF Mark, N. Bikales, CG Overberger and G. Menges (eds.) John Wiley and Sons, New York, 1985, 906 pages, US $240,£ 170, ISBN 0-471-89540-7. Elsevier1987.

57. Bains, A.; Cao, Y. M.; Kly, S.; Wulff, J. E.; Moffitt, M. G., Controlling structure and function of polymeric drug delivery nanoparticles using microfluidics. *Mol. Pharm.* **2017,** *14*, 2595–2606.

58. Schabas, G.; Wang, C. W.; Oskooei, A.; Yusuf, H.; Moffitt, M. G.; Sinton, D., Formation and shear-induced processing of quantum dot colloidal assemblies in a multiphase microfluidic chip. *Langmuir* **2008,** *24*, 10596-10603.

59. Wang, C. W.; Oskooei, A.; Sinton, D.; Moffitt, M. G., Controlled Self-Assembly of Quantum Dot-Block Copolymer Colloids in Multiphase Microfluidic Reactors. *Langmuir* **2010,** *26*, 716-723.

60. Wang, C. W.; Sinton, D.; Moffitt, M. G., Flow-Directed Block Copolymer Micelle Morphologies via Microfluidic Self-Assembly. *J. Am. Chem. Soc.* **2011,** *133*, 18853-18864.

61. Wang, C. W.; Bains, A.; Sinton, D.; Moffitt, M. G., Flow-Directed Assembly of Block Copolymer Vesicles in the Lab-on-a-Chip. *Langmuir* **2012,** *28*, 15756-15761.

62. Wang, C. W.; Sinton, D.; Moffitt, M. G., Morphological Control via Chemical and Shear Forces in Block Copolymer Self-Assembly in the Lab-on-Chip. *ACS Nano* **2013,** *7*, 1424-1436.

63. Wang, C. W.; Bains, A.; Sinton, D.; Moffitt, M. G., Flow-Directed Loading of Block Copolymer Micelles with Hydrophobic Probes in a Gas-Liquid Microreactor. *Langmuir* **2013,** *29*, 8385-8394.

64. Xu, Z. Q.; Yan, B.; Riordon, J.; Zhao, Y.; Sinton, D.; Moffitt, M. G., Microfluidic Synthesis of Photoresponsive Spool-Like Block Copolymer Nanoparticles: Flow-Directed Formation and Light-Triggered Dissociation. *Chem. Mater.* **2015,** *27*, 8094-8104.

65. Xu, Z. Q.; Lu, C. H.; Riordon, J.; Sinton, D.; Moffitt, M. G., Microfluidic Manufacturing of Polymeric Nanoparticles: Comparing Flow Control of Multiscale Structure in Single-Phase Staggered Herringbone and Two-Phase Reactors. *Langmuir* **2016,** *32*, 12781-12789.

66. Bains, A.; Cao, Y. M.; Moffitt, M. G., Multiscale Control of Hierarchical Structure in Crystalline Block Copolymer Nanoparticles Using Microfluidics. *Macromol. Rapid Comm.* **2015,** *36*, 2000-2005.

67. Bains, A.; Wulff, J. E.; Moffitt, M. G., Microfluidic synthesis of dye-loaded polycaprolactone-block-poly (ethylene oxide) nanoparticles: Insights into flow-directed loading and in vitro release for drug delivery. *J. Colloid Interf. Sci.* **2016,** *475*, 136-148.

68. Bains, A.; Moffitt, M. G., Effects of chemical and processing variables on paclitaxel-loaded polymer nanoparticles prepared using microfluidics. *J. Colloid Interf. Sci.* **2017,** *508*, 203-213.

69. Capretto, L.; Carugo, D.; Mazzitelli, S.; Nastruzzi, C.; Zhang, X. L., Microfluidic and lab-on-a-chip preparation routes for organic nanoparticles and vesicular systems for nanomedicine applications. *Adv. Drug Deliver. Rev.* **2013,** *65*, 1496-1532.

70. Morikawa, Y.; Tagami, T.; Hoshikawa, A.; Ozeki, T., The Use of an Efficient Microfluidic Mixing System for Generating Stabilized Polymeric Nanoparticles for Controlled Drug Release. *Biol. Pharm. Bull.* **2018,** *41*, 899-907.

71. Rizis, G.; van de Ven, T. G. M.; Eisenberg, A., Crystallinity-driven morphological ripening processes for poly(ethylene oxide)-block-polycaprolactone micelles in water. *Soft Matter* **2014,** *10*, 2825-2835.